Acta Crystallographica Section B
Structural Science
ISSN 0108-7681

Structures and the oxygen deficiency of tetragonal and monoclinic zirconium oxide nanoparticles

Masatomo Yashima[a]* and Shin Tsunekawa[b]

[a]Department of Materials Science and Engineering, Interdisciplinary Graduate School of Science and Engineering, Tokyo Institute of Technology, 4259 Nagatsuta-cho, Midori-ku, Yokohama, Kanagawa 226-8502, Japan, and [b]Institute for Materials Research, Tohoku University, Katahira 2-1-1, Aoba-ku, Sendai, Miyagi 980-8577, Japan

Correspondence e-mail: yashima@materia.titech.ac.jp

Received 27 April 2005
Accepted 24 September 2005

The crystal structure of zirconium oxide nanoparticles was refined by the Rietveld analysis of synchrotron X-ray powder diffraction data measured at 298 K. In the nanoparticles, two phases of tetragonal $ZrO_{2-\delta}$ (average particle size: 11 ± 2 nm) and monoclinic ZrO_2 (average particle size: 24 ± 4 nm) existed, where the weight fractions were estimated to be 84.9 and 15.1 wt%, respectively. The structural refinement suggests that the tetragonal $ZrO_{2-\delta}$ has an oxygen deficiency [$\delta = 0.031\,(7)$] and that the monoclinic $ZrO_{2-\delta}$ has less oxygen deficiency ($\delta \simeq 0$), where δ is the vacancy concentration. The monoclinic ZrO_2 has a larger unit-cell volume. The maximum-entropy method analysis indicated covalent bonding between Zr and O atoms.

1. Introduction

Pure zirconia (ZrO_2) exhibits the following phase transitions (Yashima *et al.*, 1997).

$$\underset{\text{Monoclinic}}{P2_1/c} \underset{1013\text{-}1323\ \text{K}}{\rightleftarrows} \underset{\text{Tetragonal}}{P4_2/nmc} \underset{2642\ \text{K}}{\rightarrow} \underset{\text{Cubic}}{Fm\bar{3}m} \underset{2983\ \text{K}}{\rightarrow} \text{Liquid}$$

Phase stability and particle-size dependence in pure zirconium oxides have extensively been studied by numerous researchers (Garvie, 1978; Yashima *et al.*, 1997; Chraska *et al.*, 2000; Fabris *et al.*, 2002; Tsunekawa *et al.*, 2003, 2005). Recently, Tsunekawa *et al.* (2005) indicated that the valence of Zr ions in the zirconium oxide nanocrystallites decreases with decreasing particle size, suggesting the occurrence of oxygen deficiency δ in $ZrO_{2-\delta}$ ($0 < \delta \leq 1$), where δ is the vacancy concentration. Although the nanocrystallites include both tetragonal and monoclinic phases, the oxygen deficiency of each phase has not been directly determined yet. The purpose of the present work is to determine the oxygen deficiencies in both tetragonal and monoclinic phases of a nanocrystalline sample from a precise diffraction experiment. Furthermore, we investigate the electron-density distribution of the nanosized tetragonal $ZrO_{2-\delta}$.

2. Experimental

Precursor sols were prepared from a mixture of 70 wt% zirconium(IV) propoxide 1-propanol solution and 98 wt% triethanolamine. The sols were hydrolyzed with a half volume of water in a Teflon-lined autoclave at 383 K for 24 h and then at 393 K for 120 h. A fine white powder was separated from the mother solution by a centrifuge and rinsed several times with ethanol. In order to obtain zirconium oxide nanocrystallites, the ethanol sol was dried in air on a quartz plate at 398 K for 22 h. The transmission electron microscopic observations (Tsunekawa *et al.*, 2005) revealed that the zirconium oxide nanocrystallites have average particle sizes of 11 ± 2 nm and 24 ± 4 nm in diameter, respectively, in the tetragonal and monoclinic phases. Chemical analysis by inductively coupled plasma (ICP) optical emission spectrometry indicated a small amount of hafnium and the average chemical composition of $(Zr_{0.994}Hf_{0.006})O_{2-\delta}$.

We performed synchrotron X-ray powder diffraction experiments of a zirconium oxide nanocrystalline sample using the multiple-detector system (Toraya *et al.*, 1996) installed at the BL-4B$_2$ experimental station of the Photon Factory, High Energy Accelerator Research Organization (KEK), Japan. The experimental set up consisted of a bending-magnet light source, a double-crystal Si(111) monochromator, a focusing cylindrical mirror, and a multiple-detector system with Ge(111) analyzer crystals, Soller slits and scintillation counters (Toraya *et al.*, 1996). Monochromated (1.20200 Å) X-rays were utilized. Powder diffraction data from the sample at 298 K in air were collected in asymmetric flat-specimen reflection geometry with a fixed incident angle

Table 1
Experimental details.

	Tetragonal $ZrO_{2-\delta}$ phase	Monoclinic ZrO_2 phase
Crystal data		
Chemical formula	$(Zr_{0.994}Hf_{0.006})O_{2-\delta}$ [δ = 0.031 (7)]	$(Zr_{0.994}Hf_{0.006})O_{2.00}$
M_r	123.246	123.746
Space group	$P2_1/c$	$P4_2/nmc$
a, b, c (Å)	3.58651 (8), 3.58651 (8), 5.16658 (15)	5.1313 (13), 5.1857 (13), 5.3248 (14)
α, β, γ (°)	90.0, 90.0, 90.0	90.0, 99.34 (2), 90.0
V (Å^3)	66.458 (3)	139.81 (6)
Z	2	4
D_x (Mg m^{-3})	6.1589	5.879
Radiation type	Monochromated synchrotron X-ray	Monochromated synchrotron X-ray
θ range (°)	$2\theta_{min}$ = 11.0, $2\theta_{max}$ = 140.0, θ = 7.0 (fixed)	$2\theta_{min}$ = 11.0, $2\theta_{max}$ = 140.0, θ = 7.0 (fixed)
Temperature (K)	298	298
Specimen form, colour	Flat circular sheet (particle morphology: plate-like), white	Flat circular sheet (particle morphology: plate-like), white
Specimen size (mm)	12 mm in diameter, 0.5 mm in height	12 mm in diameter, 0.5 mm in height
Data collection		
Diffractometer	A multiple-detector system with Ge(111) analyzer crystals, Soller slits and scintillation counters (Toraya *et al.*, 1996)	A multiple-detector system with Ge(111) analyzer crystals, Soller slits and scintillation counters (Toraya *et al.*, 1996)
Data collection method	Specimen mounting: packed powder pellet; mode: reflection; scan method: step	Specimen mounting: packed powder pellet; mode: reflection; scan method: step
Absorption correction	None	None
No. of measured reflections	84	562
R_{int} in the Rietveld analysis	0.0087	0.0080
R_{int} in the first MPF analysis	0.0070	0.0069
Range of h, k, l	$0 \Rightarrow h \Rightarrow 5$ $0 \Rightarrow k \Rightarrow 3$ $0 \Rightarrow l \Rightarrow 8$	$-7 \Rightarrow h \Rightarrow 7$ $0 \Rightarrow k \Rightarrow 8$ $0 \Rightarrow l \Rightarrow 8$
Refinement		
R factors and goodness-of-fit in the Rietveld analysis	R_{wp} = 0.0610, R_p = 0.0465, R_e = 0.0630, goodness-of-fit = R_{wp}/R_e = 0.968	R_{wp} = 0.0610, R_p = 0.0465, R_e = 0.0630, goodness-of-fit = R_{wp}/R_e = 0.968
R factors and goodness-of-fit in the first MPF analysis	R_{wp} = 0.0607, R_p = 0.0463, R_e = 0.0630, goodness-of-fit = R_{wp}/R_e = 0.963	R_{wp} = 0.0607, R_p = 0.0463, R_e = 0.0630, goodness-of-fit = R_{wp}/R_e = 0.963
Wavelength of incident raidation (Å)	1.20200	1.20200
Excluded regions	None	None
Profile function	Split-type Pearson VII (Toraya, 1990)	Split-type Pearson VII (Toraya, 1990)
No. of parameters	57 (13 for structural parameters)	57 (13 for structural parameters)
Preferred orientation correction	None	None

Computer programs used: Rigaku software (Toraya *et al.*, 1996), *RIETAN*-2000 (Izumi & Ikeda, 2000), *VENUS* (Izumi & Dilanian, 2002).

of 7.0°. Scanning parameters were as follows: step interval 0.010°, counting time 4.5 s per step, and diffraction angle 2θ ranging from 11 to 140°.

The crystal structures of the zirconium oxide nanocrystallites were refined by the Rietveld method using the computer program *RIETAN*-2000 (Izumi & Ikeda, 2000). Since the enhancement in the asymmetric scan mode (Toraya *et al.*, 1993) is not implemented in *RIETAN*-2000, the observed intensity data were modified by multiplying $2/[1 + \{\sin\alpha/\sin(2\theta - \alpha)\}]$, where α is the fixed incident angle to obtain data equivalent with those measured in the symmetric scan mode. The peak shape was assumed to be a split-type Pearson VII-type function (Toraya, 1990). The cut-off value was 7.00 × (full width at half-maximum). The background was approximated by a 12-parameter polynomial in $2\theta^n$, where n has values between 0 and 11. The n parameters were simultaneously refined with the unit-cell, zero-point, scale, profile-shape and crystal structural parameters. An electron-density distribution of the tetragonal zirconium oxide nanocrystallites was investigated by the maximum-entropy method (MEM) with the structure factors obtained by Rietveld analysis. There were 77 structure factors. The MEM calculations were carried out using the computer program *PRIMA* (Izumi & Dilanian, 2002) with 64 × 64 × 91 pixels. To confirm the validity of the MEM analysis we performed an MEM-based whole pattern fitting (MPF: Izumi & Dilanian, 2002) with the structure factors obtained by the Fourier transform of the MEM electron-density distribution (see Table 1).[1]

3. Results and discussion

All the reflections were indexed with the tetragonal (space group $P4_2/nmc$; Yashima *et al.*, 1994) and monoclinic (space group $P2_1/c$; Yashima *et al.*, 1995) phases (Fig. 1). The isotropic harmonic model was used for all the atomic displacement parameters. In a preliminary Rietveld analysis, the occupancy factors of the O atoms in the tetragonal and monoclinic phases were refined independently. The occupancy factor of the O atoms of the monoclinic phase was 1.12 (4), thus it was fixed at 1.00 in the final refinement. This suggests that the monoclinic phase has no oxygen deficiency. The calculated synchrotron X-ray powder diffraction profile agreed well with that observed (Fig. 1 and Table 2). Fig. 2(*a*) shows the refined crystal structure of the tetragonal phase. The axial ratio c/a_F was 1.0186, which is a little smaller than that (1.0204) obtained by the extrapolation of the c/a_F values of metastable bulk tetragonal zirconia solid solutions (Yoshimura *et al.*, 1990). Here a_F denotes the lattice parameter based on the pseudo-fluorite lattice, *i.e.* $a_F = 2^{1/2} \cdot a$, where a is the lattice parameter of the tetragonal phase. The fractional z coordinate of the O atom in the tetragonal phase was refined to be 0.2041 (2), which is a little larger than that obtained for bulk tetragonal zirconia at high temperatures (Aldebert & Traverse, 1985). These differences could be ascribed to a nano-sized effect. The displacement of the O atom along the c axis of 0.237 (1) Å was confirmed, leading to two different values of the bond lengths between the cation and the anion [R = 2.3562 (6) Å and r = 2.0805 (5) Å in Fig. 2*a*]. The unit-cell volume of the monoclinic phase was larger than that of the tetragonal phase (Table 2). This is also the case in the bulk zirconia (Frey *et al.*, 1990) and its solid solutions (Yashima *et al.*, 1995).

The occupancy factor of the O atom in the tetragonal phase was refined to be 0.984 (4). This suggests that the tetragonal $ZrO_{2-\delta}$ has an oxygen deficiency [δ = 0.031 (7)]. The corresponding chemical formula of the tetragonal phase was $ZrO_{2-\delta}$ [δ = 0.031 (7)]. On the contrary, the monoclinic phase did not have an oxygen deficiency within experimental error. These results suggest that the phase transition from monoclinic to

[1] Supplementary data for this paper are available from the IUCr electronic archives (Reference: OG5013). Services for accessing these data are described at the back of the journal.

Table 2
Refined crystal parameters and reliability factors in the Rietveld and MPF analyses of synchrotron X-ray powder diffraction data for $(Zr_{0.994}Hf_{0.006})O_{2-\delta}$ nanoparticles (298 K).

Symmetry, average particle size, chemical formula	Site	Occupancy	Fractional coordinate			Atomic displacement parameters B
			x	y	z	
Tetragonal†	$Zr_{0.994}Hf_{0.006}$ 2(a)	1	0	0	0	$B_t(Zr_{0.994}Hf_{0.006})$ = 0.385 (1) Å^2
$P4_2/nmc$	O 4(d)	0.984 (4)	0	1/2	0.2041 (2)	B_t(O) = 0.934 (17) Å^2
11 ± 2 nm	$a = b$ = 3.58651 (8) Å, c = 5.16658 (15) Å, V = 132.916 (6) Å^3‡					
$(Zr_{0.994}Hf_{0.006})O_{2-\delta}$ δ = 0.031 (7)	R_I = 0.87%, R_F = 0.61% (Rietveld); R_I = 0.70%, R_F = 0.44% (first MPF)					
Monoclinic†	$Zr_{0.994}Hf_{0.006}$ 4(e)	1	0.2274 (7)	0.0369 (6)	0.2825 (7)	= $B_t(Zr_{0.994}Hf_{0.006})$
$P2_1/c$	O1 4(e)	1	−0.024 (6)	0.224 (2)	0.497 (5)	= B_t(O)
24 ± 4 nm	O2 4(e)	1	0.532 (5)	0.826 (4)	0.337 (3)	= B_t(O)
$(Zr_{0.994}Hf_{0.006})O_{2.00}$	a = 5.1313 (13), b = 5.1857 (13), c = 5.3248 (14) Å, β = 99.34 (2)°, V = 139.81 (6) Å^3					
	R_I = 0.80%, R_F = 0.54% (Rietveld); R_I = 0.69%, R_F = 0.41% (first MPF)					

R_{wp} = 6.10%, R_p = 4.65%, R_e = 6.30%, goodness-of-fit = R_{wp}/R_e = 0.968 (Rietveld); R_{wp} = 6.07%, R_p = 4.63%, R_e = 6.30%, goodness-of-fit = R_{wp}/R_e = 0.963 (first MPF) † Weight fractions of tetragonal and monoclinic phases are estimated to be 0.849 and 0.151, respectively. ‡ Reduced cell volume for the pseudo-fluorite-type structure.

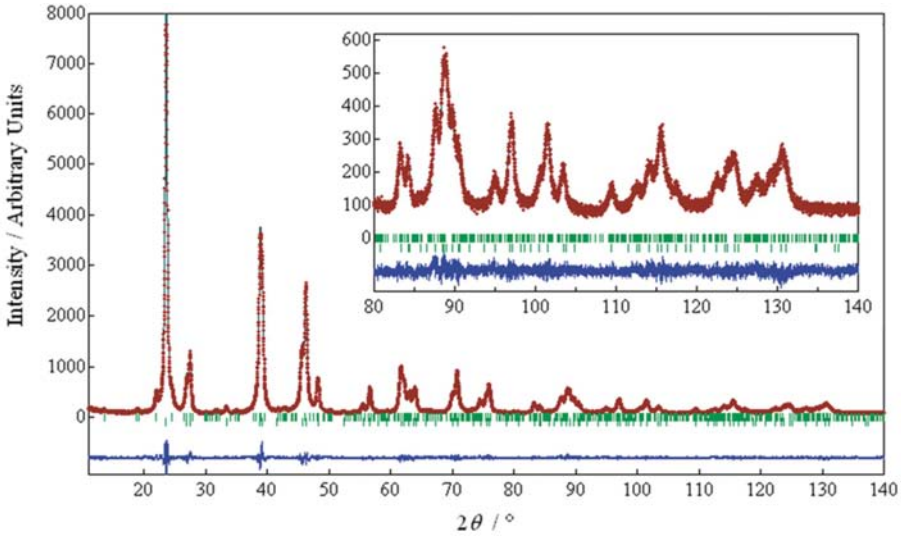

Figure 1
Rietveld refinement of the synchrotron X-ray powder diffraction data of the zirconium oxide nanoparticles. A magnified view of the peak profile in the 2θ range from 80 to 140° is inserted. Red points and the green line denote the observed and calculated intensities, respectively. The difference between the observed and calculated intensities is drawn by a blue line below the profile. Up and down green short verticals denote the calculated peak positions of the monoclinic and tetragonal phases, respectively.

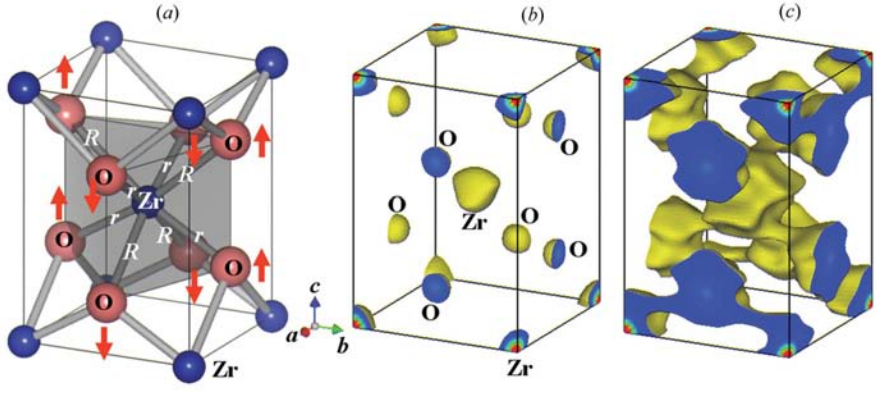

Figure 2
Refined crystal structure (*a*) and equi-electron-density surfaces at 10 (*b*) and 1 Å^{-3} (*c*) of the tetragonal zirconium oxide nanoparticles. The two bond lengths between the cation and anion are R = 2.3562 (6) and r = 2.0805 (5) Å. The arrows represent the displacements of the O atoms along the c axis [0.237 (1) Å].

tetragonal in zirconium oxide nanocrystallites could be caused by the oxygen deficiency as is the tetragonal to cubic transition in the nanocrystallites (Tsunekawa *et al.*, 2005). Similar behavior has been reported in the tetragonal–cubic phase boundary in bulk crystals of stabilized zirconia: the tetragonal–cubic phase boundary decreases with increasing oxygen defect concentration (Yashima *et al.*, 1996).

The MEM electron-density map shown in Fig. 2(*b*) is consistent with the refined crystal structure of the tetragonal phase. The electrons are located at the positions of the Zr and O atoms. No extra peaks are observed in the MEM electron-density map. The MEM density map also suggests the anisotropic distribution of the cation, which could be ascribed to the thermal motion or static disorder. Larger and smaller distributions of electrons exist around the cation along the longer and shorter Zr—O bonds, respectively (Fig. 2*b*). The MEM density map in Fig. 2(*c*) indicates covalent bonding between Zr and O atoms. The bond with the shorter Zr—O length, r, has stronger bonding, while the bond with the longer distance, R, has weaker bonding.

We are grateful to Dr T. Ashino of Analytical Research Core for Advanced Materials of the IMR, Tohoku University, for his chemical analysis of zirconium oxides. We also thank Mr S. Kobayashi, W. Nakamura, Y. Ando and T. Tsuji (Tokyo Institute of Technology) for experimental assistance. Financial supports were provided partly by the Grant-in-Aids for Scientific Research (B) of the Ministry of Education, Culture, Sports, Science and Technology, Japan. This study was carried out under the PAC No. 2002 G074, 2002 G229, 2003 G039, 2003 G220, 2004 G046 and 2004 G223. Fig. 2

was drawn with the VENUS program made by Drs. R. A. Dilanian and F. Izumi.

References

Aldebert, P. & Traverse, J.-P. (1985). *J. Am. Ceram. Soc.* **68**, 34–40.

Chraska, T., King, A. H. & Berndt, C. C. (2000). *Mater. Sci. Eng. A*, **286**, 169–178.

Fabris, S., Paxton, A. T. & Finnis, M. W. (2002). *Acta Mater.* **50**, 5171–5178.

Frey, F., Boysen, H. & Voigt, T. (1990). *Acta Cryst.* B**46**, 724–730.

Garvie, R. C. (1978). *J. Phys. Chem.* **82**, 218–224.

Izumi, F. & Dilanian, R. A. (2002). *Recent Research Developments in Physics*, Vol. 3, Part II, pp. 699–726. Trivandrum, India: Transworld Research Network.

Izumi, F. & Ikeda, T. (2000). *Mater. Sci. Forum*, **321–324**, 198–203.

Toraya, H. (1990). *J. Appl. Cryst.* **23**, 485–491.

Toraya, H., Huang, T. C. & Wu, Y. (1993). *J. Appl. Cryst.* **26**, 774–777.

Toraya, H., Hibino, H. & Ohsumi, K. (1996). *J. Synchrotron Rad.* **3**, 75–84.

Tsunekawa, S., Asami, K., Ito, S., Yashima, M. & Sugimoto, T. (2005). *Appl. Surf. Sci.* **252**, 1651–1656.

Tsunekawa, S., Ito, S., Kawazoe, Y. & Wang, J.-T. (2003). *Nano Lett.* **3**, 871–875.

Yashima, M., Hirose, T., Katano, S., Suzuki, Y., Kakihana, M. & Yoshimura, M. (1995). *Phys. Rev. B*, **51**, 8018–8025.

Yashima, M., Kakihana, M., Ishii, K., Ikuma, Y. & Yoshimura, M. (1996). *J. Mater. Res.* **11**, 1410–1420.

Yashima, M., Kato, T., Kakihana, M., Gulgun, M. A., Matsuo, Y. & Yoshimura, M. (1997). *J. Mater. Res.* **12**, 2575–2583.

Yashima, M., Sasaki, S., Kakihana, M., Yamaguchi, Y., Arashi, H. & Yoshimura, M. (1994). *Acta Cryst.* B**50**, 663–672.

Yoshimura, M., Yashima, M., Noma, T. & Somiya, S. (1990). *J. Mater. Sci.* **25**, 2011–2016.